Simulation of transition dynamics to high confinement in fusion plasmas

Nielsen, Anders Henry; Xu, G. S.; Madsen, Jens; Naulin, Volker; Rasmussen, Jens Juul; Wan, B. N.

Published in:
Physics Letters A

Link to article, DOI:
10.1016/j.physleta.2015.10.004

Publication date:
2015

Document Version
Peer reviewed version

Simulation of transition dynamics to high confinement in fusion plasmas

A H. Nielsen[a], G.S. Xu[b], J. Madsen[a], V. Naulin[a], J. Juul Rasmussen[a], B.N. Wan[b]

[a] *Department of Physics, Technical University of Denmark, Fysikvej, DK-2800 Kgs.-Lyngby, Denmark*
[b] *Institute of Plasma Physics, Chinese Academy of Sciences, Hefei 230031, People's Republic of China*

Abstract

The transition dynamics from the low (L) to the high (H) confinement mode in magnetically confined plasmas is investigated using a first-principles four-field fluid model. Numerical results are in agreement with measurements from the Experimental Advanced Superconducting Tokamak - EAST. Particularly, the slow transition with an intermediate dithering phase is well reproduced at proper parameters. The model recovers the power threshold for the L-H transition as well as the decrease in power threshold switching from single to double null configuration observed experimentally. The results are highly relevant for developing predictive models of the transition, essential for understanding and optimizing future fusion power reactors.

Keywords: L-H transition, fluid simulations, Braginskii equations, turbulence and flows
PACS: 52.25.Fi, 52.35.Ra, 52.55.Fa, 05.70.Fh

1. Introduction

An outstanding issue in magnetic fusion research is the understanding and prediction of the transition between the Low (L-mode) and High (H-mode) confinement mode. Although the H-mode is routinely achieved in a multitude of magnetic confinement devices, since its first observation more than 30 years ago, the transition still lacks (full) theoretical explanation and predictive modelling. The L-H transition represents a characteristic feature of complex nonlinear systems, were an abrupt transition between two states is

encountered in response to variation of some "control" parameter. Examples are transport bifurcations: the transition from dominating convective cell transport to global circulation in Rayleigh-Benard convection[1], and the formation of transport barriers by zonal flows, e.g., the earth's polar vortex[2, 3].

The L-mode is characterized by relatively flat pressure profiles and significant turbulent particle and energy transport across the Last Closed Flux Surface (LCFS) into the region of open field lines - the Scrape-Off Layer (SOL). The H-mode is characterized by a pedestal of elevated pressure just inside the LCFS and a quiescent transport into the SOL leading to improved confinement. Generally, the generation and sustainment of global flows is observed to be a key ingredient in the transition[4, 5]. The transition behaviour can vary from very abrupt transitions to slow transitions with intermediate (I) phases[6, 5]. Here, the I-phase refers to the transition phase between the L- and H-mode, characterized by strong quasi-periodic bursts of plasma into the SOL (the I-phase is also referred to as the dithering phase or limit-cycle oscillations (LCO)); see, e.g., [7, 8, 9, 10, 11, 12, 13]. The H-mode is of essential importance for the operation and success of ITER - the next generation international fusion experiment. To achieve the goal of ignition, ITER will rely on low power access to the H-mode.

Recent experiments with advanced diagnostics provide detailed spatially and temporally information about the L-I-H transition dynamics. These experiments demonstrate in detail that the control of the L-H transition depends on the gradients in the edge region, see e.g. [14, 7, 8].

Concurrent with the improved experimental diagnostics, new modelling approaches have been developed for the simulation of the coupled Edge-SOL dynamics. Two important ingredients on the way towards improved understanding of the SOL dynamics have been to abandon the distinction between fluctuations and profiles and the usage of flux driven systems[15, 16, 17].

The L-H transition is connected with the build-up of Zonal Flows (ZF), suspected to be triggered by turbulent Reynolds Stress (RS) and finally being sustained as Mean Flows (MF) driven by the steepened ion pressure gradient. The interaction between these players is complex and in principle may contain many elements, from electromagnetic perturbations to three-dimensional effects including details of the geometry. Parts of the transition dynamics have been reproduced by heuristic zero and more recently one-dimensional predator-prey type modelling, with one or two feedback loops

acting on disparate time-scales (fast and slow), see, e.g., [18, 19, 20, 21].

The robustness of the L-H transition indicates a basic mechanism that we believe is represented in the interaction of the two-dimensional electrostatic turbulence with the self-consistently developing profiles, including the interaction between ion pressure and flow, specifically. Important is also the role of the Edge-SOL coupling anchoring initial gradients to the LCFS. We use the first principle fluid model HESEL[22, 23] to simulate experimental observations from the Experimental Advanced Superconducting Tokamak - EAST. The HESEL model includes the elements discussed above and has enabled us to perform detailed studies of the L-I-H dynamics for parameters determined by experiment with the only exception being the ramp-up power rate in the edge region, a parameter not directly obtainable from the experiments.

2. Model

HESEL is an energy conserving four-field model based on the Braginskii equations[24] governing the dynamics of a quasi-neutral, simple plasma. It describes interchange-driven, low-frequency turbulence in a plane perpendicular to the magnetic field at the outboard midplane. In the limit of constant ion pressure the model reduces to the ESEL model, which has successfully modeled fluctuations and profiles in JET[25], MAST[26], EAST[27] and TCV[28]. The HESEL model includes the transition from the confined region to the SOL and the full development of the profiles across the LCFS. The model is solved in a local slab geometry with inhomogeneous toroidal magnetic field approximated by $B(r) = B_0 R/(R + a + r)$, where a, R, r and B_0 are the minor, major radius, the radial coordinate in the local slab and the on-axes magnetic field strength, respectively. In the Bohm-normalization

the model equations read:

$$\frac{d}{dt}n + n\mathcal{K}(\phi) - \mathcal{K}(p_e) = -\nabla\cdot(n\boldsymbol{u}_R) - \frac{n}{\tau_n}, \tag{1}$$

$$\frac{d^0}{dt}w + \{\nabla\phi, \nabla p_i\} - \mathcal{K}(p_e + p_i) = \Lambda_w, \tag{2}$$

$$\Lambda_w = \eta\nabla^2 w - \frac{w}{\tau_w} + \frac{\rho_s}{L_\parallel}\left[1 - \exp\left(\Phi - \frac{\langle\phi\rangle}{\langle T_e\rangle}\right)\right],$$

$$\frac{3}{2}\frac{d}{dt}p_e + \frac{5}{2}p_e\mathcal{K}(\phi) - \frac{5}{2}\mathcal{K}\left(\frac{p_e^2}{n}\right) = \nabla\cdot\left(\chi_{e\perp}\nabla T_e\right) - \frac{5}{2}\nabla\cdot(p_e\boldsymbol{u}_R)$$

$$- \boldsymbol{u}_R\cdot\nabla p_i - \frac{T_e}{\tau_{p_e}}, \tag{3}$$

$$\frac{3}{2}\frac{d}{dt}p_i + \frac{5}{2}p_i\mathcal{K}(\phi) + \frac{5}{2}\mathcal{K}\left(\frac{p_i^2}{n}\right) - p_i\mathcal{K}(p_e + p_i) = \nabla\cdot\left(\chi_{i\perp}\nabla T_i\right) - \frac{5}{2}\nabla\cdot(p_i\boldsymbol{u}_R)$$

$$+ \boldsymbol{u}_R\cdot\nabla p_i - \frac{p_i}{\tau_{p_i}} + p_i\Lambda_w, \tag{4}$$

where n is particle density, $w = \nabla^2\phi + \nabla^2 p_i$ is the generalized vorticity, ϕ is the electrostatic potential, and p_e and p_i are electron and ion pressure, respectively. Temperatures are defined by $T_{i,e} = p_{i,e}/n$. Material derivatives and the magnetic field curvature operator are defined as $\frac{d}{dt} = \frac{\partial}{\partial t} + \frac{1}{B}\hat{\boldsymbol{z}}\times\nabla\phi\cdot\nabla$, $\mathcal{K} = \nabla\left(\frac{1}{B}\right)\cdot\hat{\boldsymbol{z}}\times\nabla$, except in the generalized vorticity equation where the material derivative $\frac{d^0}{dt}$ is taken with a constant magnetic field. Friction forces enter through the drift velocity $\boldsymbol{u}_R = -D(1 + T_i/T_e)\nabla\ln n$, where D is the neo-classical Pfirsch-Schlüter diffusion coefficient[25]. η denotes the neo-classical viscosity coefficient, and $\chi_{e\perp}$ and $\chi_{i\perp}$ are the neo-classical, perpendicular electron and ion heat conduction coefficients, respectively. Losses due to advection along magnetic field lines in the SOL region are represented by the damping rates τ_n^{-1}, τ_w^{-1}, and $\tau_{p_i}^{-1}$ and parallel electron heat conduction by $\tau_{p_e}^{-1}$. The effect of sheath currents at material surfaces on which magnetic field lines in the SOL region terminate, is approximated by an effective sheath dissipation term entering the vorticity Eq. (2), where $L_\parallel$ is the connection length, $\Phi = log(\sqrt{m_i/(2\pi m_e)})$ and $\langle\cdot\rangle$ denotes a poloidal average. In the inner part of the closed field line region the fluid fields are forced towards profiles reflecting toroidal equilibrium.

The generalized vorticity is the manifestation of the polarization current in the model and describes charge separation due to the inertia in the ion

response to changes in the $\boldsymbol{E} \times \boldsymbol{B}$ and diamagnetic drifts. The generalized vorticity is responsible for driving the MF related to the pressure gradient and is essential for setting up the edge transport barrier supporting the pressure pedestal in the H-mode. Simulations with only the $\boldsymbol{E} \times \boldsymbol{B}$ fluid vorticity do not reveal a L-H transition.

We simulate experimental observations from the 2012 L-I-H transition campaign at EAST. These experiments employed the Gass Puff Images (GPI) diagnostics[8, 29] measuring the intensity of the emission from excited neutrals, the HeI-line, in the plane perpendicular to the local magnetic field. The emission is directly related to the electron pressure[30]. Using high speed cameras and correlation techniques it is possible to derive e.g. velocity profiles from the propagation of perturbations. For comparing the experimental observations to numerical simulations we employ a synthetic GPI diagnostics in the simulations which calculate the emission intensity according to: $S_n \propto n_e n_n f(n_e, T_e)$[30]. Here, f is the helium excitation coefficient and n_n is the neutral gas density profile calculated at each point in time from neutral particles penetrating from the outer SOL and getting depleted by ionisation.

The collision and parallel damping rate coefficients for all simulations presented in this paper are calculated using parameters for the plasma in EAST shot 41362. We use the LCFS values of electron density $n_0 = 1.5 \times 10^{19}\,\mathrm{m}^{-3}$ and electron temperature $T_{e0} = 20\,\mathrm{eV}$ and distance from the LCFS to the limiter shadow $\Delta_{SOL} = 2.4\,\mathrm{cm}$. Furthermore, we use $B_0 = 2.0\,\mathrm{T}$, safety factor $q = 4.5$, $R = 2.0\,\mathrm{m}$ and $a = 0.5\,\mathrm{m}$. In the simulations the non-constant power input in EAST is emulated by ramping up the reference ion temperature: $T_{i0}(t) = T_{i0}(0) + (T_{i0}(t_{\max}) - T_{i0}(0))sin(\frac{\pi}{2}\frac{t}{t_{\max}})$ where $T_{i0}(0) = 20\,\mathrm{eV}$ and $T_{i0}(t_{\max}) = 60\,\mathrm{eV}$. The prescribed ion pressure profile at the inner radial boundary is adjusted accordingly. All ion temperature dependent diffusion and parallel damping coefficients are recalculated at each point in times as the ion temperature is ramped up.

3. Results

Figures 1 and 2 display the time evolution of radial profiles and two integrated quantities from EAST shot 41362 and HESEL, respectively. The profiles are obtained by averaging over the poloidal measurement/simulation direction. The L- and H-modes are clearly recognized at the being and end of the plots. Between these two states we observe a number of I-phases, where bursts of plasma are quasi-periodically being ejected from the edge region

far into the SOL, significantly flattening the intensity profiles (Figs. 1a and 2a), increasing the fluctuation levels (Figs. 1b and 2b), and breaking down of the pressure gradient (Figs. 1c and 2c). In the numerical simulations the observed number of I-phases is basically determined by the ion temperature ramp up rate t_{max}, a slightly slower (faster) ramp-up rate will result in more (less) I-phases. The duration of the I-phase as well as the number of bursts are here matched between simulation and experiment. Note also that the period of the bursts is increasing as we approach the H-mode transition, both in experiment and simulation.

The D_α signal, Fig. 1d, is obtained in the EAST divertor region. It is a measure of the amount of hot plasma, which originates from perpendicular turbulent transport processes at the outboard midplane into the SOL and subsequently transported to the divertor by parallel flows. The D_α intensity shows a similar evolution as the GPI intensity in the I-phase, but is lagging the fluctuations in the other signals consistent with the SOL parallel transport time from the out-board mid-plane to the divertor. In Fig. 2d the evolution of the integrated parallel particle flux is taken as a proxy for the D_α signal in Fig. 1d. By construction it lacks the time delay seen in the experimental data but otherwise shows similar features.

The evolution of the experimentally observed poloidal velocity profile in Fig. 1e and the corresponding Reynolds stress (RS) profile, Fig. 1f, show I-phase oscillations, while in the H-mode velocity fluctuations and RS signals are significantly reduced. We note, that measurements of velocity fields, by means of correlation techniques applied to propagating turbulence visible in the GPI signals, fails in H-mode as the turbulence in the signal is too weak to correlate upon, see Fig. 1b. Numerically, we obtain these two quantities directly from the $E\times B$ velocities (Figs. 2e and 2f). The transport barrier in H-mode is sustained by a significant poloidal flow, not detectable by the experimental GPI as mentioned above. In Fig. 2g we finally show the evolution of the density profile, which is observed to closely follow the GPI intensity profile dynamics, accounting for the folding with the neutral gas profile.

A close inspection of the individual cycles in Figs. 1 and 2 reveals three distinct phases. The first phase is quiescent with nearly no fluctuations. It is followed by a second phase with increased fluctuations which dominate the dynamics. In the last phase the pressure gradient is expelled from the edge region into the SOL. The SOL is depleted of plasma and finally the pressure gradient across the LCFS re-establishes. Disappearance of the turbulent fluctuations is accompanied by the generation of a sheared zonal flow (ZF)

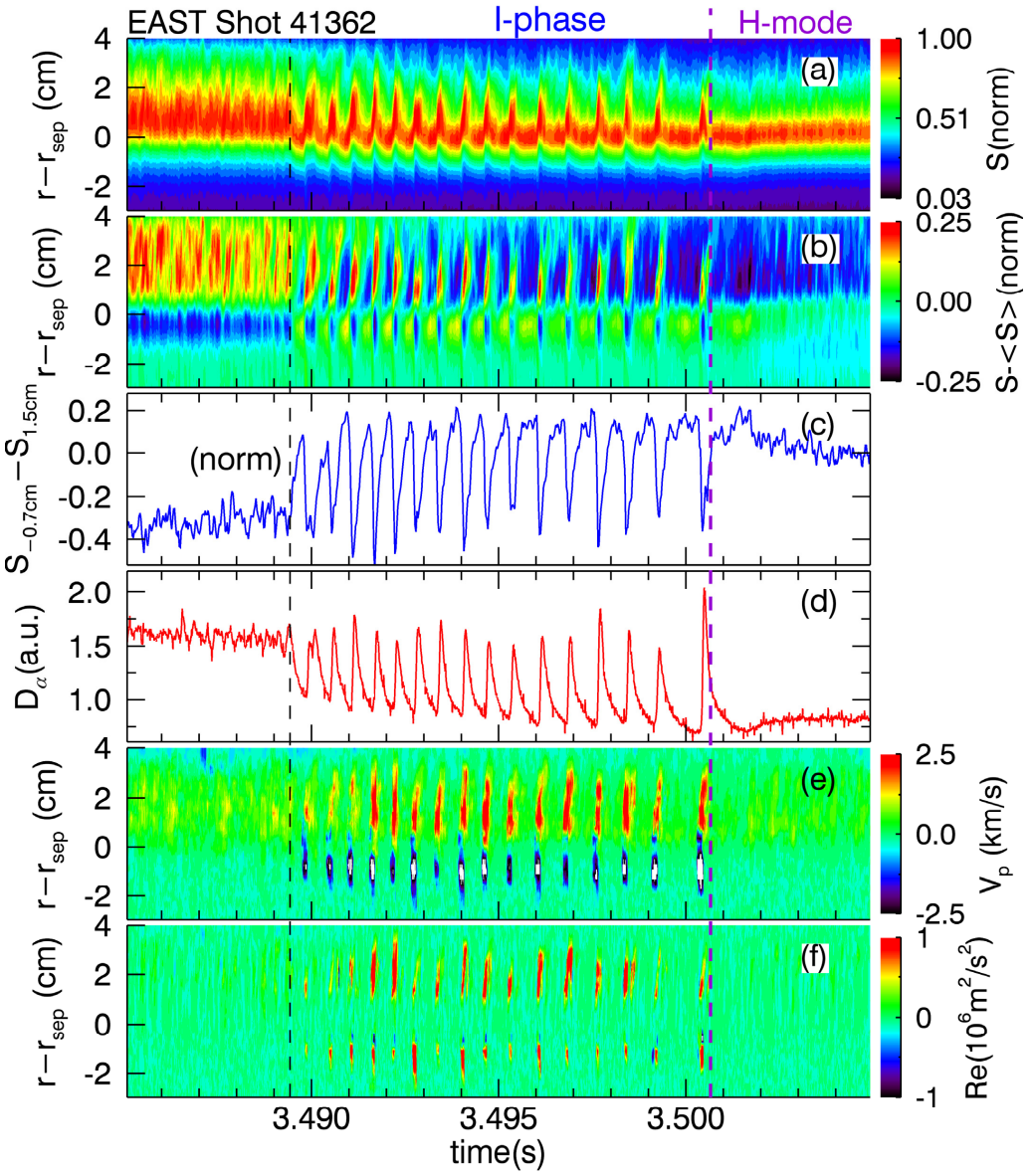

Figure 1: EAST shot no. 41362 with input power slowly ramped up revealing the essential features of the L-I-H transition. The frames show measurements from the confined region ($r < 0$) and the region with open field lines - the SOL ($r > 0$). a) The emission intensity of the HeI line, S, b) the fluctuation level of S, c) the difference in the relative GPI emission intensity between radial positions $r = -7$ mm and $r = 15$ mm, d) the D_α emission from the outer divertor region, e) poloidal flow velocity from GPI, f) turbulence-driven Reynolds stress with fluctuations in the perpendicular velocities derived from GPI.

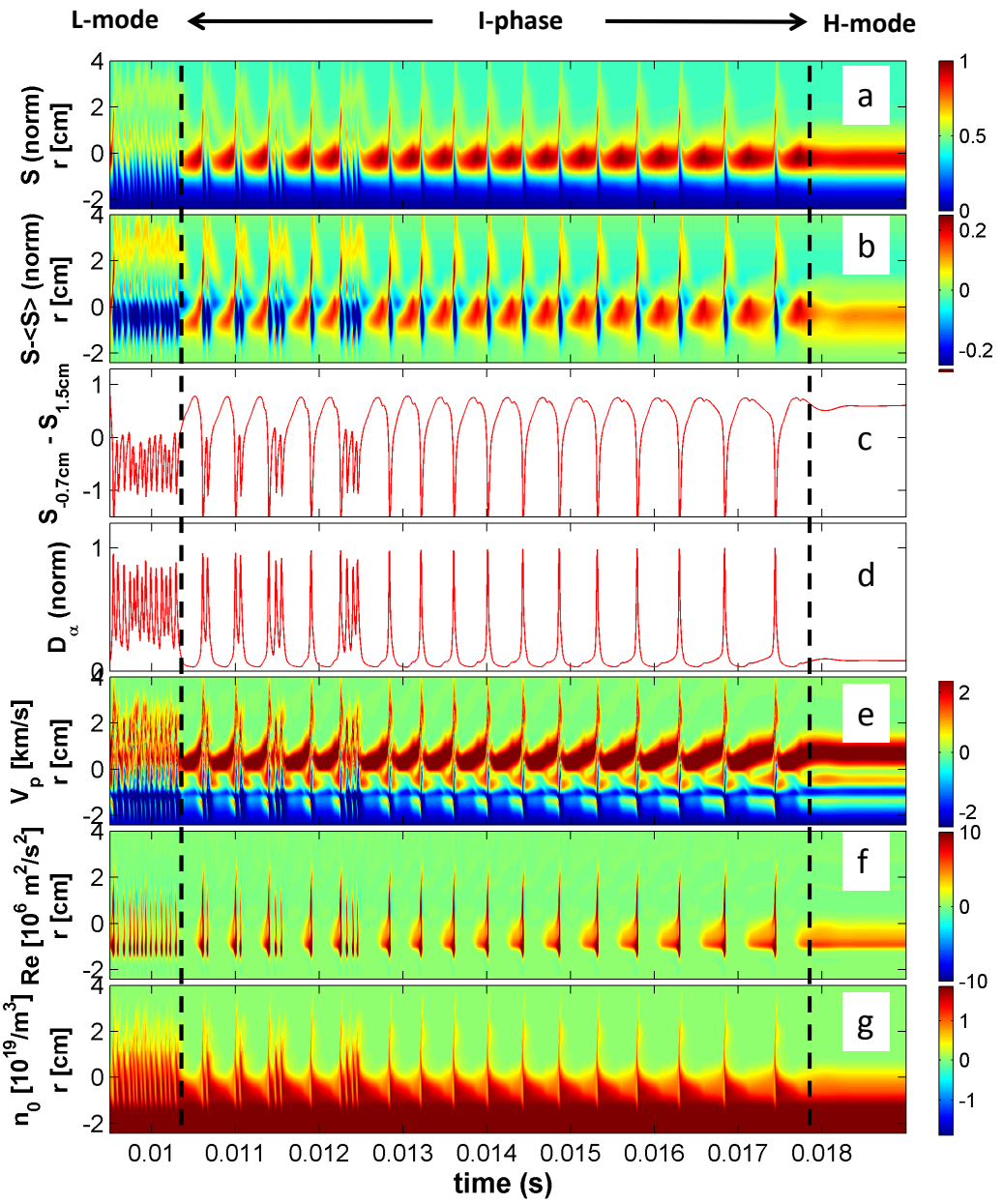

Figure 2: HESEL simulation for plasma parameters of EAST shot no 41362 similar to Fig. 1. a) to c) derived from synthetic GPI signal, d) integrated parallel particle loss term as a proxy to divertor D_α, e) and f) derived from $E\times B$ velocities, g) displays the electron density profile not accessible from GPI.

through the RS. A strongly enhanced RS and significant Reynolds work, not shown here, coincide with the termination of the burst, where a poloidal flow is rapidly re-established. The generated poloidal flow is later in parts sustained by the ion pressure gradient induced mean flow (MF), but will decay gradually. In the decay phase the RS slowly increases again, but if the MF is not strong enough to sustain the barrier, this leads towards the next burst and the cycle is closed. If, on the other hand, the MF grows strong enough a stable high confinement state is entered. Thus, the I-phase appears at sub critical heat fluxes. As the input power increases the length of the dithering cycles increases in line with building up the ion pressure gradient and mean flow, until the system is able to enter the H-mode. The quiet periods during the I-phase thus resemble the H-mode, but with the MF not yet strong enough to fully sustain it.

The L-H-like transitions observed in the simulations are robust and have been obtained for a broad range of parameters. Different types of transitions have been observed ranging from fast (μs) transitions to slow (ms) transitions with the intermediate I-phase. In agreement with experimental observations[8] L-I-L transitions have also been observed when the power input is slightly lower than the critical power. Figure 3a shows an L-H transition without an I-phase, using a faster ramp-up of the ion pressure, $t_{\max} = 2.61\,\mathrm{ms}$. As the ion pressure is ramp-down a clear hysteresis is observed with a H-L transition occurring for an ion pressure at a value corresponding to a decrease in ion temperature at constant density by approximately 10 eV compared to the L-H threshold. After the H-L transition the heat flux reverts to the same level as before the transition, a behaviour routinely observed in experiments[5, 31]. The total heat flux across the LCFS into the SOL can be estimated from the HESEL simulations to be 1.2 MW for the LH transition. Here we assume that the heat flux crossing the LCFS has an axisymmetric distribution and originates from a region 30 degree poloidally above and below the outboard midplane. This heat flux is in close agreement to the estimated experimental input power of about 1.0 MW for this particular shot[8].

The simulations also provide insight into the general scaling of the L-H transition threshold power. Figure 3b show a series of HESEL simulations for different reference particle densities n_0. We observe that the transition threshold power increases at increasing particle density, as observed in the high density branch of the L-H transition threshold power[5]. Commonly observed is also a fast increase of the L-H power threshold at lower densi-

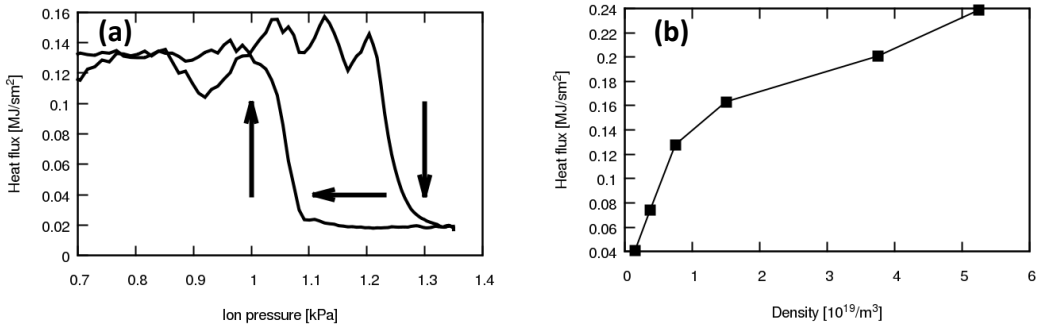

Figure 3: HESEL simulations displaying a) the total heat flux across the LCFS as a function of the ion pressure at the LCFS during a transition, b) heat flux across the LCFS at the transition for different densities.

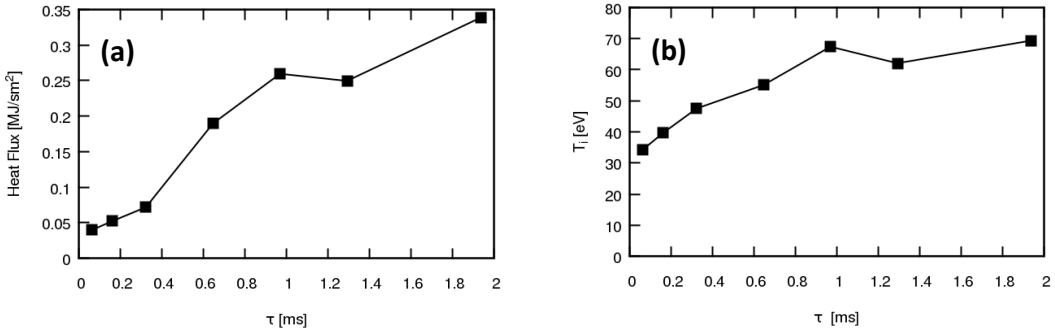

Figure 4: HESEL simulations displaying a) the total heat flux across the LCFS and b) the ion temperature at the transition as a function of a characteristic parallel advection loss time, $\tau = L_{\parallel}/c_{s0}$.

ties, leading to a well-defined density with minimal power necessary to enter H-mode. In these experiments electrons are dominantly heated centrally. However, it was recently demonstrated that the ion heat channel plays the key role in the L-H transition[32], and the ion energy flux crossing the LCFS depends on the energy coupling between electrons and ions over the whole plasma volume. This coupling is weaker at low densities which may explain the increase in the electron power input threshold at low density. When the power input is directly through the ions one should not expect to find a roll-over of the threshold power at a specific density as demonstrated in [32]. Our simulation results agree with this observation.

Figure 4 shows the total heat flux across the LCFS and the corresponding

ion temperature at the L-H transition as a function of a characteristic parallel advection loss time, $\tau = L_\parallel / c_{s0}$, c_{s0} being the ion sound speed at LCFS. As τ decreases we observed a strong nearly linear decrease in heat flux, a feature in agreement with experimental observations. A significant reduction in the threshold was first observed at MAST[33] but have later been confirmed in other devices, e.g., NSTX and ASDEX Upgrade[34] and EAST[35]. Also, recent observations from TCV report a reduction in power threshold as the X-point is moved downward thus decreasing $L_\parallel$[36].

4. Conclussions

To the best of our knowledge this is the first modelling of the L-H transition with direct comparisons to experimental observations reproducing many details of the transition behaviour with key parameters obtained from experiment. The model appears to include the necessary and essential ingredients for the transition behaviour, but is not a fully predictive model as, e.g., details of a toroidal plasma is not modelled. The results presented here form an essential step connecting the zero- and one-dimensional heuristic transition models with predictive models and thus the full set of toroidal plasma dynamics. Bridging this gab is essential for the ITER experiment, which relies on controlled H-mode access.

5. acknowledgments

This work was supported by the National Magnetic Confinement Fusion Science Program of China under Contracts No. 2011GB107001, by National Natural Science Foundation of China under Contracts No. 11422546 and the Sino-Danish Center for Education and Research (SDC). JM was supported by an EFDA fusion researcher fellowship (WP11-FRF-RISOE/MADSEN).

[1] H. Mori, Y. Kuramoto, Dissipative structures and chaos, 2nd Edition, Springer, Berlin, 1998.

[2] D. G. Dritschel, M. E. McIntyre, Multiple jets as pv staircases: The phillips effect and the resilience of eddy-transport barriers, Journal of the Atmospheric Sciences 65 (3) (2008) 855–874. doi:10.1175/2007JAS2227.1.

[3] M. E. Mcintyre, Chapter 1 The atmospheric waveturbulence jigsaw, World Scientific Book, Edited P. H. Diamond and X. Garbet and P. Ghendrih and Y. Sarazin, 2014.
URL http://citeseerx.ist.psu.edu/viewdoc/summary?doi=10.1.1.295.4841

[4] F. Wagner, G. Becker, K. Behringer, D. Campbell, A. Eberhagen, W. Engelhardt, G. Fussmann, O. Gehre, J. Gernhardt, G. von Gierke, G. Haas, M. Huang, F. Karger, M. Keilhacker, O. Kluber, M. Kornherr, K. Lackner, G. Lisitano, G. G. Lister, H. M. Mayer, D. Meisel, E. R. Muller, H. Murmann, H. Niedermeyer, W. Poschenrieder, H. Rapp, H. Rohr, F. Schneider, G. Siller, E. Speth, A. Stabler, K. H. Steuer, G. Venus, O. Vollmer, Z. Yu, Regime of improved confinement and high beta in neutral-beam-heated divertor discharges of the asdex tokamak, Physical Review Letters 49 (19) (1982) 1408–1412.

[5] F. Wagner, A quarter-century of h-mode studies, Plasma Physics and Controlled Fusion 49 (12B) (2007) B1–B33. doi:10.1088/0741-3335/49/12B/S01.

[6] H. Zohm, Dynamic behavior of the l-h transition, Physical Review Letters 72 (2) (1994) 222–225.

[7] G. S. Xu, B. N. Wan, H. Q. Wang, H. Y. Guo, H. L. Zhao, A. D. Liu, V. Naulin, P. H. Diamond, G. R. Tynan, M. Xu, R. Chen, M. Jiang, P. Liu, N. Yan, W. Zhang, L. Wang, S. C. Liu, S. Y. Ding, First evidence of the role of zonal flows for the l-h transition at marginal input power in the east tokamak., Physical Review Letters 107 (12) (2011) 125001:1.

[8] G. Xu, L. Shao, S. Liu, H. Wang, B. Wan, H. Guo, P. Diamond, G. Tynan, M. Xu, S. Zweben, V. Naulin, A. H. Nielsen, J. Juul Rasmussen, N. Fedorczak, P. Manz, K. Miki, N. Yan, R. Chen, B. Cao, L. Chen, L. Wang, W. Zhang, X. Gong, Study of the lih transition with a new dual gas puff imaging system in the east superconducting tokamak, Nuclear Fusion 54 (1) (2014) 013007. doi:10.1088/0029-5515/54/1/013007.

[9] L. Schmitz, L. Zeng, T. L. Rhodes, J. C. Hillesheim, E. J. Doyle, R. J. Groebner, W. A. Peebles, K. H. Burrell, G. Wang, Role of zonal flow predator-prey oscillations in triggering the transition to h-mode confinement, Physical Review Letters 108 (15) (2012) 155002. doi:10.1103/PhysRevLett.108.155002.

[10] L. Schmitz, L. Zeng, T. L. Rhodes, J. C. Hillesheim, W. A. Peebles, R. J. Groebner, K. H. Burrell, G. R. McKee, Z. Yan, G. R. Tynan, P. H. Diamond, J. A. Boedo, E. J. Doyle, B. A. Grierson, C. Chrystal, M. E. Austin, W. M. Solomon, G. Wang, The role of zonal flows and predator-prey oscillations in triggering the formation of edge and core transport barriers, NUCLEAR FUSION 54 (7) (2014) 073012. doi:10.1088/0029-5515/54/7/073012.

[11] J. Cheng, J. Q. Dong, K. Itoh, L. W. Yan, M. Xu, K. J. Zhao, W. Y. Hong, Z. H. Huang, X. Q. Ji, W. L. Zhong, D. L. Yu, S. I. Itoh, L. Nie, D. F. Kong, T. Lan, A. D. Liu, X. L. Zou, Q. W. Yang, X. T. Ding, X. R. Duan, Y. Liu, H.-A. Team, Dynamics of low-intermediate-high-confinement transitions in toroidal plasmas, Physical Review Letters 110 (26) (2013) 265002. doi:10.1103/PhysRevLett.110.265002.

[12] T. Kobayashi, K. Itoh, T. Ido, K. Kamiya, S. I. Itoh, Y. Miura, Y. Nagashima, A. Fujisawa, S. Inagaki, K. Ida, K. Hoshino, Spatiotemporal structures of edge limit-cycle oscillation before l-to-h transition in the jft-2m tokamak, Physical Review Letters 111 (3) (2013) 035002. doi:10.1103/PhysRevLett.111.035002.

[13] T. Kobayashi, K. Itoh, T. Ido, K. Kamiya, S. I. Itoh, Y. Miura, Y. Nagashima, A. Fujisawa, S. Inagaki, K. Ida, N. Kasuya, K. Hoshino, Dynamics of edge limit cycle oscillation in the jft-2m tokamak, NUCLEAR FUSION 54 (7) (2014) 1. doi:10.1088/0029-5515/54/7/073017.

[14] R. J. Groebner, D. M. Thomas, R. D. Deranian, Evidence for edge gradients as control parameters of the spontaneous high-mode transition, Physics of Plasmas, Phys Plasmas 8 (6) (2001) 2722–2730. doi:10.1063/1.1365104.

[15] O. E. Garcia, R. A. Pitts, J. Horacek, A. H. Nielsen, W. Fundamenski, J. P. Graves, V. Naulin, J. J. Rasmussen, Turbulent transport in the tcv sol, Journal of Nuclear Materials 363-365 (2007) 575–580. doi:10.1016/j.jnucmat.2006.12.063.

[16] V. Naulin, Turbulent transport and the plasma edge., Journal of Nuclear Materials 363-365 (2007) 24.

[17] Y. Sarazin, P. Beyer, X. Garbet, S. Benkadda, Anomalous transport and complexity in plasma turbulence, Physica Scripta T 84 (2000) 14–17.

[18] X. Wu, G. Xu, B. Wan, J. J. Rasmussen, V. Naulin, A. H. Nielsen, One-dimensional modelling of limit-cycle oscillation and h-mode power scaling, NUCLEAR FUSION 55 (5). doi:10.1088/0029-5515/55/5/053029.

[19] E. J. Kim, P. H. Diamond, Zonal flows and transient dynamics of the l-h transition, Physical Review Letters 90 (18) (2003) 185006/1–185006/4.

[20] M. Dam, M. Brns, J. Juul Rasmussen, V. Naulin, G. Xu, Bifurcation analysis and dimension reduction of a predator-prey model for the l-h transition, Physics of Plasmas 20 (10) (2013) 102302. doi:10.1063/1.4823719.

[21] K. Miki, P. H. Diamond, O. D. Guercan, G. R. Tynan, T. Estrada, L. Schmitz, G. S. Xu, Spatio-temporal evolution of the l - i - h transition, Physics of Plasmas 19 (9) (2012) 092306. doi:10.1063/1.4753931.

[22] A. H. Nielsen, J. Madsen, G. Xu, V. Naulin, J. Juul Rasmussen, N. Yan, 2d fluid simulations of interchange turbulence with ion dynamics, Conference Paper 40th European Physical Society Conference on Plasma Physics, Espoo, Finland (2013) http://ocs.ciemat.es/EPS2013PAP/pdf/P5.173.pdf.

[23] J. Madsen, A. H. Nielsen, V. Naulin, J. Juul Rasmussen, G. Xu, B. Wan, 2d interchange model including ion dynamics, Paper in preparation.

[24] S. Braginskii, Transport processes in a plasma, In Review of Plasma Physics, (ed. Leontovich, M. A.). New York, NY: Consultants Bureau Vol. 1 (1965) 205–311.

[25] W. Fundamenski, O. E. Garcia, V. Naulin, R. A. Pitts, A. H. Nielsen, J. J. Rasmussen, J. Horacek, J. P. Graves, J. E. contributors, Dissipative processes in interchange driven scrape-off layer turbulence, Nuclear Fusion 47 (5) (2007) 417–433. doi:10.1088/0029-5515/47/5/006.

[26] F. Militello, P. Tamain, W. Fundamenski, A. Kirk, V. Naulin, A. H. Nielsen, Experimental and numerical characterization of the turbulence in the scrape-off layer of mast, Plasma Physics and Controlled Fusion 55 (2) (2013) 025005. doi:10.1088/0741-3335/55/2/025005.

[27] N. Yan, A. H. Nielsen, G. Xu, V. Naulin, J. Juul Rasmussen, J. Madsen, H. Q. Wang, S. C. Liu, W. Zhang, L. Wang, B. N. Wan, Statistical

characterization of turbulence in the boundary plasma of east, Plasma Physics and Controlled Fusion 55 (11) (2013) 115007. doi:10.1088/0741-3335/55/11/115007.

[28] O. E. Garcia, V. Naulin, A. H. Nielsen, J. Juul Rasmussen, Turbulence and intermittent transport at the boundary of magnetized plasmas, Physics of Plasmas 12 (6) (2005) 062309. doi:10.1063/1.1925617.

[29] S. C. Liu, L. M. Shao, S. J. Zweben, G. Xu, H. Y. Guo, B. Cao, H. Q. Wang, L. Wang, N. Yan, S. B. Xia, W. Zhang, R. Chen, L. Chen, S. Y. Ding, H. Xiong, Y. Zhao, B. N. Wan, X. Z. Gong, X. Gao, New dual gas puff imaging system with up-down symmetry on experimental advanced superconducting tokamak, Review of Scientific Instruments 83 (12) (2012) 123506. doi:10.1063/1.4770122.

[30] R. Maqueda, G. Wurden, D. Stotler, S. Zweben, B. LaBombard, J. Terry, J. Lowrance, V. Mastrocola, G. Renda, D. D'Ippolito, J. Myra, N. Nishino, Gas puff imaging of edge turbulence (invited), Review of Scientific Instruments 74 (3) (2003) 2020–2026. doi:10.1063/1.1535249.

[31] D. M. Thomas, R. J. Groebner, K. H. Burrell, T. H. Osborne, T. Carlstrom, The back transition and hysteresis effects in diii-d, PLASMA PHYSICS AND CONTROLLED FUSION 40 (5) (1998) 707–712. doi:10.1088/0741-3335/40/5/028.

[32] F. Ryter, L. B. Orte, B. Kurzan, R. M. McDermott, G. Tardini, E. Viezzer, M. Bernert, R. Fischer, Experimental evidence for the key role of the ion heat channel in the physics of the lh transition, Nuclear Fusion 54 (8) (2014) 083003. doi:10.1088/0029-5515/54/8/083003.

[33] H. Meyer, P. G. Carolan, N. J. Conway, G. F. Counsell, G. Cunningham, A. R. Field, A. Kirk, K. G. McClements, M. Price, D. Taylor, the MAST Team, Improved h-mode access in connected dnd in mast, Plasma Physics and Controlled Fusion 47 (6) (2005) 843.
URL http://stacks.iop.org/0741-3335/47/i=6/a=008

[34] H. Meyer, P. Carolan, G. Conway, G. Cunningham, L. Horton, A. Kirk, R. Maingi, F. Ryter, S. Saarelma, J. Schirmer, W. Suttrop, H. Wilson, M. Team, A. U. Team, N. Team, H-mode physics of near double null plasmas in mast and its applications to other tokamaks, Nuclear Fusion,

Nucl. Fusion, Nucl Fusion, Nuclear Fusion Journal of Plasma Physics and Thermonuclear Fusion, Nucl. Fus 46 (1) (2006) 64–72.

[35] Z. X. Liu, X. Gao, S. C. Liu, S. Y. Ding, T. Y. Xia, T. Zhang, S. B. Zhang, Y. M. Wang, X. Han, J. G. Li, Y. Yang, Y. X. Jie, B. L. Ling, E. Team, H-mode power threshold and confinement in a molybdenum wall with different magnetic configurations on the east tokamak, NUCLEAR FUSION 53 (7) (2013) 1. doi:10.1088/0029-5515/53/7/073041.

[36] Y. Martin, R. Behn, I. Furno, B. Labit, H. Reimerdes, T. Team, H-mode access during plasma current ramp-up in tcv, NUCLEAR FUSION 54 (11) (2014) 114006. doi:10.1088/0029-5515/54/11/114006.